A Robust Design for Ultra Reliable Ambient Backscatter Communication Systems

Yu Zhang, Bin Li, *Senior Member, IEEE*, Feifei Gao, *Senior Member, IEEE*, and Zhu Han, *Fellow, IEEE*

***Abstract*—Backscatter communications have been considered as one of the key technologies in the Internet of Things (IoT) applications. In this paper, we consider a multitag ambient backscatter system, where the multiple tags can harvest radio frequency (RF) energy from the power station and backscatter the RF signals to the reader for data transmission. In order to guarantee the throughput requirements, we aim to maximize the minimum user rate among all the tags by jointly optimizing the backscatter time allocation and power reflection coefficient. Channel state information (CSI) mismatch is taken into account in our proposed optimization problem, which leads to a robust chance-constrained optimization problem. To deal with the nonconvex chance constraints, we propose two safe approximation methods: 1) Bernstein-type-inequality and 2) conditional value-at-risk (CVaR), applying to the Gaussian distribution and arbitrary distribution of channel estimation errors, respectively. In addition, we develop an alternating optimization algorithm to obtain the optimal value of minimum throughput. Finally, simulation results reveal that the CVaR-based method outperforms the Bernstein-type-inequality-based method for the non-Gaussian channel estimation error.**

***Index Terms*—Backscatter communication, chance constraint, conditional value-at-risk (CVaR), distributionally robust optimization, Internet of Things (IoT), optimization.**

Manuscript received April 7, 2019; revised May 17, 2019 and June 9, 2019; accepted June 26, 2019. Date of publication July 1, 2019; date of current version October 8, 2019. This work was supported in part by the National Natural Science Foundation of China under Grant 61531011, Grant 61831013, Grant 61771274, and Grant 61701124, in part by the Beijing Municipal Natural Science Foundation under Grant 4182030 and Grant L182042, in part by the Research and Development Project of the Science, Technology and Innovation Commission of Shenzhen Municipality under Grant JCYJ20180306170617062, in part by the U.S. Multidisciplinary University Research Initiative (MURI) Air Force Office of Scientific Research (AFOSR) MURI under Grant 18RT0073, Grant NSF CNS-1717454, Grant CNS-1731424, Grant CNS-1702850, and Grant CNS-1646607, in part by the Sichuan Science and Technology Program under Grant 2019YJ0105, and in part by the China Scholarship Council under Grant 201806210090. *(Corresponding author: Feifei Gao.)*

Y. Zhang is with the Department of Automation, Tsinghua University, Beijing 100084, China (e-mail: z-y16@mails.tsinghua.edu.cn).

B. Li is with the College of Electrical Engineering, Sichuan University, Chengdu 610065, China, and also with the Key Laboratory of Wireless Power Transmission of Ministry of Education, Sichuan University, Chengdu 610065, China (e-mail: bin.li@scu.edu.cn).

F. Gao is with the Department of Automation, Tsinghua University, Beijing 100084, China, also with the Institute for Artificial Intelligence, Tsinghua University, Beijing 100084, China, also with the Beijing National Research Center for Information Science and Technology, Beijing 100084, China, and also with the Key Laboratory of Digital TV System of Guangdong Province and Shenzhen City, Research Institute of Tsinghua University in Shenzhen, Shenzhen 518057, China (e-mail: feifeigao@ieee.org).

Z. Han is with the Department of Electrical and Computer Engineering, University of Houston, Houston, TX 77004 USA, and also with the Department of Computer Science and Engineering, Kyung Hee University, Seoul 446-701, South Korea (e-mail: zhan2@uh.edu).

Digital Object Identifier 10.1109/JIOT.2019.2925843

I. Introduction

As THE Internet of Things (IoT) grows, tens of billions of sensor nodes will be connected in the future. It is significantly challenging to maintain such a large-scale network since the embedded batteries in massive IoT devices need to be replaced or recharged when they exhausted. Making the IoT devices consuming as little power as possible while transmitting and collecting data is very important. One possible solution is to take advantage of backscatter communications, which allows the IoT devices to transmit data by reflecting an incident radio frequency (RF) signals. The power consumed in backscatter transmitter is about 11 μW for its operation [1], which is extraordinarily lower than that of conventional wireless systems. Moreover, the backscatter communication systems (BCSs) can harvest energy from a dedicated or ambient RF source to power the integrate circuit, which can be regarded as a special wireless powered communication network (WPCN). The difference is that the BCS using the backscatter mode to transmit data [2].

Generally, BCSs can be divided into three types based on the architecture [3]: 1) *monostatic* BCSs (MBCSs); 2) *bistatic* BCSs (BBCSs); and 3) *ambient* BCSs (ABCSs). RF identification (RFID) system is a typical MBCS, which includes a reader and a tag [4]. The reader in MBCSs can be acted as an RF source as well as a backscatter receiver. Specially, the reader sends the query signals (QSs) to the tag periodically. The tag can be activated by the QSs within the interrogation ranges. The information signals of tag are modulated onto the QSs and reflected back to the reader. The MBCSs usually operate in short-range RFID applications due to the signal loss from reader to tag. In order to overcome the limited range of MBCSs, Kimionis *et al.* [5] proposed a BBCS, which is formed by a separate carrier emitter and backscatter receiver. The carrier emitter generating the RF signals can be placed close to the tag to increase the power-link budget gains [6], [7]. From the experimental measurement, a carrier emitter-to-tag distance of 5.5 m, a carrier emitter-to-reader distance of 100 m can be achieved [5]. Different from the BBCSs, ABCSs utilize the ambient RF sources, such as TV, Wi-Fi, and cellular transmissions rather than the dedicated RF sources as in BBCS to power the tag [8], which can avoid the maintenance of batteries and dedicated power infrastructures.

Backscatter communication is a popular topic in recent years, which attracts a growing number of researchers studying the performance of the BCSs. Acquiring channel state information (CSI) is of great importance in the performance

analysis of BCSs. Channel estimation in BCSs can be different from that in traditional point-to-point communications. Designing the training sequence is supposed to consider both the forward and backscatter link as well as their correlation in BCSs. Zhang *et al.* [9] presented a training-sequences-aided linear minimum mean square error (LMMSE) channel estimation method for the multiple-input multiple-output (MIMO) RFID systems, which exploited the inherent orthogonal characteristic of the optimal training scheme to reduce the estimation complexity. In BBCSs, the direct path interference from carrier emitter to reader can be easily eliminated since the carrier emitter RF signals are usually known. For the reader, it simply needs to acquire the CSI of the compound channel, e.g., the product of the forward and backscatter link. The least square (LS) estimation method can be adopted to estimate the compound channel [7]. However, it is challenging to use the channel estimation method based on training sequences for ABCSs due to the unknown ambient RF source. Ma *et al.* [10] proposed a blind estimation method for ABCSs without any extra pilot sequences. Through designing an expectation maximization (EM)-based estimator, the channel parameters can be iteratively obtained. Mishra and Larsson [11] proposed a novel LS estimator to estimate the forward and backscatter links between reader and tags. They also jointly optimize the number of orthogonal pilots and energy allocation for the channel estimation process. In addition, the channel estimation between tag and tag can be found in [12].

No matter what kinds of channel estimation methods are used, the channel estimation errors always cannot be avoided. Most related works assume the availability of perfect CSI in the performance of BCSs [2], [13], which is not practical. The resource allocation may be mismatched under the assumption of perfect CSI for the system design in BCSs, so that the throughput requirements cannot be guaranteed all the time [14]–[16]. In consideration of CSI mismatch, there are two main research aspects. One is assuming the distribution of errors are known, such as the Gaussian distribution [11], [17]. The other is that the errors are uncertain and can be chosen from some (bounded) set, which can lead to a worst-case-based optimization problem [18], [19].

Motivated by the aforementioned facts, we propose a chance-constrained optimization problem to maximize the minimum user rate for BCSs with consideration of the imperfect CSI. The contributions of this paper can be summarized as follows.

1) We formulate the robust chance-constrained optimization problem by jointly optimizing the backscatter time and power reflection coefficient with two outage-based constraints: a) the probability that the throughput of each tag exceeds a certain threshold is higher than a predetermined level and b) the probability that the harvested energy at each tag is above the consumed energy is greater than a predefined value.
2) We first consider the channel estimation error as the Gaussian distribution. To tackle the probabilistic constraints, we adopt the safe approximation method: Bernstein-type-inequality, which is based on the large deviation inequalities for complex Gaussian quadratic forms [20], [21].
3) Then we consider a more practical scenario, in which the reader has no prior knowledge of the distribution of errors except for the first and second-order statistics. We use another safe approximation method: conditional value-at-risk (CVaR), which is regarded as the tightest convex approximation for chance constraints [22], [23]. Particularly, motivated by the recent progress on the distributionally robust optimization in [24]–[26], we adopt the worst-case distribution of the CVaR to approximate the chance constraints, which leads to a more tractable reformulation. Simulation results show that CVaR-based method outperforms the Bernstein-type-inequality-based method for the non-Gaussian channel estimation errors.

The rest of this paper is organized as follows. In Section II, we describe the multitag ambient backscatter system model. Section III gives the formulation of the robust chance constrained optimization problem. In Section IV, a Bernstein-type-inequality safe approximation method is introduced to solve the chance constraint with Gaussian CSI mismatch. In addition, we use the worst-case CVaR approximation method to transform the formulated problem with uncertain CSI mismatch to a semi-definite programming (SDP) problem. In Section V, we design an alternating optimization algorithm for the transformed tractable nonconvex problem. The simulation results of the two proposed safe approximation methods are shown in Section VI. Finally, Section VII gives the conclusion of this paper.

Notations: x, $\boldsymbol{x}$, and $\boldsymbol{X}$ represent a scalar x, a vector $\boldsymbol{x}$, and a matrix $\boldsymbol{X}$, respectively. $\sum$ and $\mathbb{E}(\cdot)$ denote the sum and expectation operation, respectively. $\log_2(\cdot)$ and $\ln(\cdot)$ denote the binary and natural logarithmic function, respectively. We use $\mathrm{Re}(\cdot)$ to denote the real part of a complex number. $|\cdot|$ and $\|\cdot\|$ denote the absolute value and Euclidean norm, respectively. We use $\mathcal{CN}(a, b)$ to denote the complex Gaussian distribution with the mean of a and variance of b. We have $\mathrm{Tr}(\cdot)$, $(\cdot)^{\mathrm{T}}$, and $(\cdot)^{\mathrm{H}}$ to denote the trace, transpose, and conjugate transpose of a matrix, respectively. $\Pr(\cdot)$ stands for the probability of a certain event. $\mathrm{vec}(\boldsymbol{A})$ represents the vector obtained by stacking the column vectors of $\boldsymbol{A}$. $\boldsymbol{I}_N$ denotes the $N \times N$ identity matrix. $\mathbb{S}^n$ denotes the sets of $n \times n$ real symmetric matrices. We write $\boldsymbol{A} \succcurlyeq 0$ to mean that $\boldsymbol{A}$ is positive semidefinite.

II. System Model

In this paper, we consider a multitag ambient backscatter system consisting of a power station (PS), a reader, and K passive tags. The PS equipped with an omnidirectional antenna can send the RF signals to the reader and all the K tags, as shown in Fig. 1. Each reader and each tag are equipped with a single antenna. The RF signals can carry information and energy simultaneously, which is called simultaneous wireless information and power transfer (SWIPT) [27]–[29]. In Fig. 2, we can see that tag can either harvest energy from the incident RF signals to power the circuit or backscatter the RF signals for data transmission. The backscatter operation is through adjusting the load impedance of the antenna. By switching

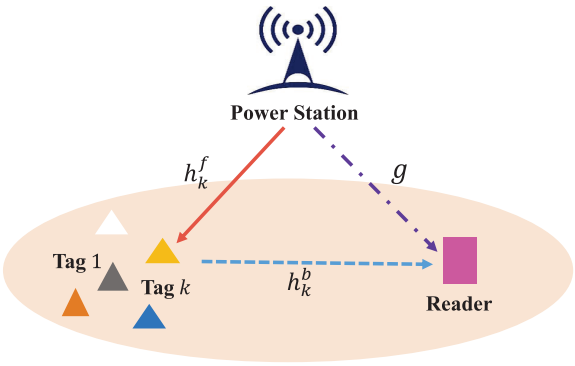

Fig. 1. Ambient backscatter system consisting of a PS, a single-antenna reader and K single-antenna tags.

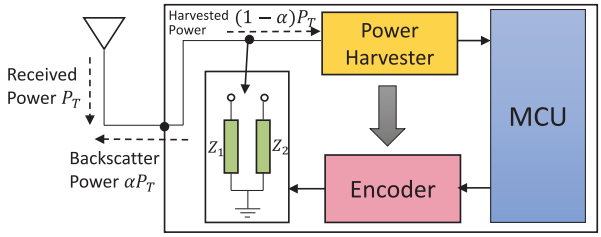

Fig. 2. Block diagram of a passive tag.

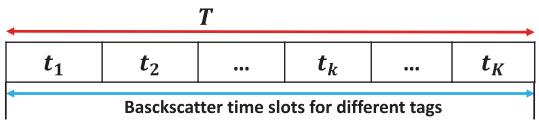

Fig. 3. Backscatter time allocation for different tags.

between two different loads Z_1 and Z_2, the tag can be shifted between absorbing and reflecting state. In the absorbing state, i.e., impedance matching, the tag reflects nothing to reader, which means the transmission of bit "0." In the reflecting state, i.e., impedance mismatching, it represents to transmit bit "1." This is known as the OOK modulation.

For the multitag ambient backscatter system, we consider a frame-based protocol. The frame duration period T is normalized to 1, i.e., $T = 1$, which is divided into K time slots, denoted by $\{t_1, t_2, \ldots, t_K\}$. Each time slot is assigned for one particular tag, as shown in Fig. 3. We denote h_k^f and h_k^b as the channel gain from the PS to the kth tag and the kth tag to the reader in Fig. 1, respectively. The channel gain from PS to the reader is represented as g. We consider the block fading channel h_k^f, h_k^b, and g, which means the channel gains remain constant during one frame but may change in other frames. The signal received by the kth tag can be expressed as

$$y_{T,k}(n) = h_k^f s(n) + n_T(n) \tag{1}$$

where $s(n)$ is the signal transmitted by the PS with power P_s and $n_T(n)$ is the noise at the tag.

The backscatter time allocation vector $\boldsymbol{t}$ is denoted as $\boldsymbol{t} = [t_1, t_2, \ldots, t_k]$. During the kth time slot of t_k, the kth tag scatters a proportion α_k ($0 < \alpha_k < 1$, power reflection coefficient) of the received RF signals to the reader. The remaining $1-\alpha_k$ power is harvested by the tag to power the circuit [30], as shown in Fig. 2. In addition, a tag can harvest energy not only during its own backscatter time slot but also from the silent time slot (other tag backscatter time slot). If the harvested energy during one frame is redundant, it can be stored to supplement the energy shortage in other frames. The total energy harvested by the kth tag during the whole frame is given by

$$E_{H,k} = \eta(1-\alpha_k)P_{T,k}t_k + \eta P_{T,i}\sum_{i=1,i\neq k}^{K} t_i \tag{2}$$

where η is energy harvesting (EH) efficiency, and $P_{T,i}$ is the power received at the kth tag during the ith time slot. Due to the unchanged channel gain h_k^f during one frame, we have $P_{T,i} = P_{T,k} = |h_k^f|^2 P_s$. In (2), the harvested energy of the kth tag consists of two parts. The first part of energy is harvested in its own backscatter time slot and the second one is harvested during the other tags' backscatter time slots. By summing these two parts together, (2) can be further simplified as

$$E_{H,k} = \eta(1-\alpha_k t_k)\left|h_k^f\right|^2 P_s. \tag{3}$$

To guarantee the tag normal operation, the harvested energy should be larger than the consumed one. Therefore, we have the EH constraint, as follows:

$$E_{H,k} \geq E_{C,k} \tag{4}$$

where $E_{C,k} = E_0 + \kappa\phi(R_k)$ is the consumed energy by the kth tag during one frame, defined as [19] and [31], and E_0 and κ are two constant terms and R_k is the transmission rate of the kth tag; $\phi(R_k)$ is the rate-dependent power consumption, which is adopted as $\phi(R_k) = R_k$ [31].

During the information transmitting phase, in the kth slot, only the kth tag operates data transmission. The signal received at the reader from the kth tag is given by

$$y_{R,k}(n) = \sqrt{\alpha_k}h_k s(n)b_k(n) + gs(n) + n_R(n) \tag{5}$$

where $h_k = h_k^f h_k^b$, and $b_k(n)$ is the information bit at the kth tag, $b_k(n) \in \{0, 1\}$ and $n_R(n)$ denotes the noise at reader, which follows the circularly symmetric complex Gaussian (CSCG) distribution, i.e., $n_R(n) \sim \mathcal{CN}(0, \sigma_R^2)$. Here, we have neglected the $n_T(n)$ term in (5) since n_T is much smaller compared with n_R. Generally, in BCSs, the noise at passive tag is negligible for the lower power consumption [32], [33].

The overall channel link $h_k = h_k^f h_k^b$ can be estimated by a training-based method, i.e., LMMSE method [9]. The channel estimation is operated at the beginning of each frame. Based on (5), the signal-to-interference-plus-noise-ratio (SINR) associated with the kth tag is given by

$$\gamma_{T,k} = \frac{\alpha_k|h_k|^2 P_s}{|g|^2 P_s + \sigma_R^2}. \tag{6}$$

Hence, the achievable throughput of the kth tag can be expressed as [14]

$$R_k = t_k \log_2\left(1 + \frac{\alpha_k|h_k|^2 P_s}{|g|^2 P_s + \sigma_R^2}\right). \tag{7}$$

III. Chance-Constrained Problem Formulation

In practice, channel estimation is a power-consuming operation for BCSs, which makes it challenging for the passive tag to send pilots or feeding back channel conditions. The accuracy of CSI cannot be guaranteed at all the time. In our proposed model, we take the imperfect CSI into consideration to make a robust design. In the imperfect case, the actual CSI of h_k and g can be expressed as [34]

$$h_k = \hat{h}_k + \Delta_{h_k} \tag{8}$$

$$g = \hat{g} + \Delta_g \tag{9}$$

where $\hat{h}_k$ and $\hat{g}$ are the estimated channels of h_k and g, respectively; Δ_{h_k} and Δ_g are the channel estimation errors of h_k and g, respectively. The pilot-based or blind estimation method can be used to obtain the estimated channel [10]–[12], [35]. The distribution of CSI error will be discussed in the following two scenarios.

1) Scenario 1-Gaussian Distribution: In most robust optimization literatures, the CSI errors are usually assumed as the CSCG distribution for system design [19], [20]. It is known that the CSI errors will tend to follow Gaussian distribution when the minimum mean square error (MMSE) channel estimation method is used for estimation [34]. As a special case, we will discuss the CSI errors of h_k and g with the zero-mean CSCG distribution in the first scenario, given by

$$\Delta_{h_k} \sim \mathcal{CN}\left(0, \sigma_{h_k}^2\right), \quad \Delta_g \sim \mathcal{CN}\left(0, \sigma_g^2\right). \tag{10}$$

2) Scenario 2-Arbitrary Distribution: In practice, we have no knowledge of the exact distribution of the CSI errors. However, it is much easier to obtain the first and second order statistics of the CSI errors compared with the exact distribution [19], [23]. Motivated by this, we define a set $\mathcal{P}$ of all distributions of Δ_{h_k} and Δ_g with the same means and (co)variances, as follows:

$$\mathcal{P} = \Big\{\mathbb{P} : \mathbb{E}_{\mathbb{P}}\big(\Delta_p\big) = \mu_p, \mathbb{E}_{\mathbb{P}}\Big[\big(\Delta_p - \mu_p\big)\big(\Delta_q - \mu_q\big)^{\mathrm{T}}\Big] = \sigma_{p,q}^2 \quad k = 1, 2, \ldots, K, \quad p, q \in \{h_k, g\}\Big\} \tag{11}$$

where μ_p and $\sigma_{p,q}^2$ are the means and (co)variances of Δ_p under distribution $\mathbb{P}$, $p, q \in \{h_k, g\}$, and $\mathbb{P}$ can be arbitrary distribution as long as its distribution meets the means and (co)variances requirements in (11).

In the above imperfect CSI model, it is hard to design the system for each tag always meeting the throughput requirements, due to the uncertainty of CSI. In practice, it is reasonable to make a robust design within the tolerance of uncertainty. Our objective is to maximize the minimum user rate among all the tags by jointly optimizing the backscatter time allocation vector $\boldsymbol{t}$ and the power reflection coefficient vector $\boldsymbol{\alpha}$ subject to the throughput and EH chance constraints. Mathematically, the optimization is formulated as follows:

$$\max_{\boldsymbol{t},\boldsymbol{\alpha},R_{\min}} \quad R_{\min} \tag{12}$$

$$\text{s.t.} \quad \Pr\left[t_k \log_2\left(1 + \frac{\alpha_k P_s |\hat{h}_k + \Delta_{h_k}|^2 |f_k|^2}{\sigma_R^2 + |\hat{g} + \Delta_g|^2 P_s}\right) \geq R_{\min}\right] \geq 1 - \epsilon_1, \forall k \tag{13}$$

$$\Pr\Big[\eta P_s |\hat{h}_k + \Delta_{h_k}|^2 (1 - \alpha_k t_k) \geq E_{C,k}\Big] \geq 1 - \epsilon_2, \forall k \tag{14}$$

$$\sum_{k=1}^{K} t_k \leq 1 \tag{15}$$

$$t_k \geq 0, \quad \forall k \tag{16}$$

$$0 \leq \alpha_k \leq 1, \quad \forall k \tag{17}$$

where $R_{\min}$ is the minimum individual throughput. Equation (13) is the throughput chance constraint, which means the throughput of each tag should meet the minimum throughput requirement with the probability at least $1 - \epsilon_1$ in the presence of channel uncertainties. Equation (14) is the EH chance constraint, which reveals the probability that the harvested energy under CSI errors is above the consumed energy $E_{C,k}$ is at least $1 - \epsilon_2$ for each tag. The chance constraints are motivated by the facts that the system can accept the outage with a tolerable probability. The backscatter time constraints are given in (15) and (16), respectively. Equation (17) gives the constraint for each tag's power reflection coefficient.

IV. Proposed Safe Approximation Methods

The robust chance-constrained optimization problem in (12)–(17) is nonconvex, which makes the problem computationally intractable. Safe approximation is commonly used in solving the chance constrained problem, which can be served as an upper bound for the original problem. In this section, we will introduce two safe approximation methods: 1) the Bernstein-type-inequality-based method and 2) CVaR method. The former is aiming at the Gaussian distribution of CSI errors, as shown in Section IV-A and the latter is for the arbitrary distribution of CSI errors, as shown in Section IV-B.

A. Bernstein-Type-Inequality-Based Method

The Bernstein-type inequality is based on a large deviation inequality for complex Gaussian quadratic forms, which bounds the probability that a sum of random variables deviates from its mean [20]. The Bernstein-type-inequality-based method can convert the complicated chance constraints into a tractable optimization problem. In order to deal with the chance constraints in (13) and (14) for Scenario 1, we use the Bernstein-type-inequality approach given in the following lemma.

Lemma 1: Let $f(\boldsymbol{x}) = \boldsymbol{x}^{\mathrm{H}}\boldsymbol{Y}\boldsymbol{x} + 2\mathrm{Re}\{\boldsymbol{x}^{\mathrm{H}}\boldsymbol{u}\}$, where $\boldsymbol{Y}$ is a complex Hermitian matrix, $\boldsymbol{Y} \in \mathbb{H}^{N\times N}$, $\boldsymbol{x} \sim \mathcal{CN}(0, \boldsymbol{I}_N)$ is a standard CSCG random vector, and $\boldsymbol{u} \in \mathbb{C}^{N\times 1}$. Then for any $\delta > 0$, we have the following statement [20]:

$$\Pr\left\{f(\boldsymbol{x}) \geq \mathrm{Tr}(\boldsymbol{Y}) - \sqrt{2\delta}\sqrt{\|\boldsymbol{Y}\|_F^2 + 2\|\boldsymbol{u}\|^2} - \delta c^+(\boldsymbol{Y})\right\} \geq 1 - e^{-\delta} \tag{18}$$

where $c^+(\boldsymbol{Y}) = \max\{\lambda_{\max}(-\boldsymbol{Y}), 0\}$ with $\lambda_{\max}(-\boldsymbol{Y})$ denotes the maximum eigenvalue of matrix $-\boldsymbol{Y}$ and $\|\cdot\|_F$ denotes the Frobenius norm.

Considering the CSI errors in Scenario 1, we define a CSI error vector, as $\boldsymbol{v}_k = [\Delta_{h_k}, \Delta_g]^{\mathrm{T}}$ with $\boldsymbol{v}_k \sim \mathcal{CN}(0, \boldsymbol{C}_k)$, where

$\boldsymbol{C}_k$ denotes the covariance matrix of $\boldsymbol{v}_k$, given by

$$\boldsymbol{C}_k = \begin{bmatrix} \sigma_{h_k}^2 & 0 \\ 0 & \sigma_g^2 \end{bmatrix}. \tag{19}$$

The derivation of $\boldsymbol{C}_k$ is presented in Appendix A. Let $\boldsymbol{v}_k = \boldsymbol{C}_k^{(1/2)}\boldsymbol{e}_k$, where $\boldsymbol{e}_k \sim \mathcal{CN}(0, \boldsymbol{I}_2)$. The chance constraint in (13) can be reformulated as

$$\Pr\{f(\boldsymbol{e}_k) \geq \chi\} \geq 1 - \epsilon_1 \tag{20}$$

where

$$f(\boldsymbol{e}_k) = \boldsymbol{e}_k^{\mathrm{H}} \boldsymbol{C}_k^{\frac{1}{2}} \boldsymbol{X}_k \boldsymbol{C}_k^{\frac{1}{2}} \boldsymbol{e}_k + 2\mathrm{Re}\left\{\boldsymbol{e}_k^{\mathrm{H}} \boldsymbol{C}_k^{\frac{1}{2}} \boldsymbol{u}\right\} \tag{21}$$

$$\boldsymbol{X}_k = \begin{bmatrix} t_k \alpha_k P_s |f_k|^2 & 0 \\ 0 & -R_{\min} P_s \end{bmatrix}, \boldsymbol{u} = \begin{bmatrix} t_k \alpha_k P_s |f_k|^2 \hat{h}_k \\ -R_{\min} P_s \hat{g} \end{bmatrix} \tag{22}$$

$$\chi = R_{\min} P_s |\hat{g}|^2 + R_{\min} \sigma_R^2 - t_k \alpha_k P_s |\hat{h}_k|^2. \tag{23}$$

The detailed derivation is provided in Appendix B. According to Lemma 1, let $\delta = -\ln \epsilon_1$ in (18), then (20) holds true if the equality

$$\mathrm{Tr}\left(\boldsymbol{C}_k^{\frac{1}{2}} \boldsymbol{X}_k \boldsymbol{C}_k^{\frac{1}{2}}\right) - \sqrt{-2\ln\epsilon_1} \sqrt{\left\|\boldsymbol{C}_k^{\frac{1}{2}} \boldsymbol{X}_k \boldsymbol{C}_k^{\frac{1}{2}}\right\|_F^2 + 2\left\|\boldsymbol{C}_k^{\frac{1}{2}} \boldsymbol{u}\right\|^2} + \ln \epsilon_1 c^+\left(\boldsymbol{C}_k^{\frac{1}{2}} \boldsymbol{X}_k \boldsymbol{C}_k^{\frac{1}{2}}\right) \geq \chi \tag{24}$$

is satisfied. Hence, the chance constraint form (20) is conservatively transformed as the deterministic form (24). However, (24) is still not the tractable constraint. We will make the further transformation by introducing two auxiliary variables θ_1, θ_2. According to the equality technique, (24) is equivalently to the following constraints:

$$\mathrm{Tr}\left(\boldsymbol{C}_k^{\frac{1}{2}} \boldsymbol{X}_k \boldsymbol{C}_k^{\frac{1}{2}}\right) - \sqrt{-2\ln\epsilon_1}\theta_1 + \ln \epsilon_1 \theta_2 \geq \chi \tag{25}$$

$$\sqrt{\left\|\boldsymbol{C}_k^{\frac{1}{2}} \boldsymbol{X}_k \boldsymbol{C}_k^{\frac{1}{2}}\right\|_F^2 + 2\left\|\boldsymbol{C}_k^{\frac{1}{2}} \boldsymbol{u}\right\|^2} \leq \theta_1 \tag{26}$$

$$\theta_2 \boldsymbol{I}_2 + \boldsymbol{C}_k^{\frac{1}{2}} \boldsymbol{X}_k \boldsymbol{C}_k^{\frac{1}{2}} \succcurlyeq \boldsymbol{0} \tag{27}$$

$$\theta_2 \succcurlyeq 0. \tag{28}$$

Moreover, (26) can be written as a second-order cone (SOC) constraint, given by

$$\left\|\begin{bmatrix} \mathrm{vec}\left(\boldsymbol{C}_k^{\frac{1}{2}} \boldsymbol{X}_k \boldsymbol{C}_k^{\frac{1}{2}}\right) \\ \sqrt{2}\boldsymbol{C}_k^{\frac{1}{2}} \boldsymbol{u} \end{bmatrix}\right\| \leq \theta_1. \tag{29}$$

Similarly, let $\Delta_{h_k} = \sigma_{h_k} e_{h_k}$, where $e_{h_k} \sim \mathcal{CN}(0, 1)$. Then the EH constraint in (14) can be transformed as

$$\Pr\left\{f\left(e_{h_k}\right) \geq \zeta_2\right\} \geq 1 - \epsilon_2 \tag{30}$$

where

$$f\left(e_{h_k}\right) = \zeta_1 |e_{h_k}|^2 + 2\mathrm{Re}\left\{e_{h_k}^{\mathrm{H}} \nu\right\} \tag{31}$$

$$\zeta_1 = \eta P_s (1 - \alpha_k t_k)\sigma_{h_k}^2, \quad \nu = \eta P_s (1 - \alpha_k t_k)\hat{h}_k \sigma_{h_k} \tag{32}$$

$$\zeta_2 = E_{C,k} - \eta P_s (1 - \alpha_k t_k)|\hat{h}_k|^2. \tag{33}$$

Using the Bernstein-type inequality in Lemma 1, the chance constraint in (30) can be conservatively transformed into the following deterministic form, given by:

$$\zeta_1 - \sqrt{2\delta_2}\sqrt{|\zeta_1|^2 + 2|\nu|^2} - \delta_2 c^+(\zeta_1) \geq \zeta_2 \tag{34}$$

where $\delta_2 = -\ln \epsilon_2$. According to Lemma 1, (30) can always hold true as long as (34) is true. Nevertheless, (34) is still not a linear constraint. We introduce two auxiliary variables ϑ_1 and ϑ_2 to transform (34) into a series of tractable constraints, given by

$$\zeta_1 - \sqrt{2\delta_2}\vartheta_1 - \delta_2 \vartheta_2 \geq \zeta_2 \tag{35}$$

$$\left\|\begin{bmatrix} \zeta_1 \\ \sqrt{2}\nu \end{bmatrix}\right\| \leq \vartheta_1 \tag{36}$$

$$\vartheta_2 + \zeta_1 \geq 0 \tag{37}$$

$$\vartheta_2 \geq 0. \tag{38}$$

Hence, after using the Bernstein-type-inequality-based method in Lemma 1, the original chance-constrained problem under Scenario 1 is reformulated as a tractable optimization problem, given by

$$P_1: \max_{\substack{\boldsymbol{t}, \boldsymbol{\alpha}, R_{\min} \\ \theta_1, \theta_2, \vartheta_1, \vartheta_2}} \quad R_{\min} \tag{39}$$

$$\text{s.t. } (15),\ (16),\ (17) \tag{40}$$

$$(25),\ (27),\ (28),\ (29) \tag{41}$$

$$(35),\ (36),\ (37),\ (38) \tag{42}$$

where (25) and (27)–(29) is the transformation of the throughput chance constraint in (13), and (35)–(38) is the equivalent transformation of EH chance constraint in (14).

B. CVaR-Based Method

In Scenario 2, the distribution of CSI errors is not exactly known. An effective way to deal with this case is to transform (12) and (14) into a distributionally robust chance constraint, given by

$$\inf_{\mathbb{P}\in\mathcal{P}} \Pr_{\mathbb{P}}\left[t_k \log_2\left(1 + \frac{\alpha_k P_s |\hat{h}_k + \Delta_{h_k}|^2 |f_k|^2}{\sigma_R^2 + |\hat{g} + \Delta_g|^2 P_s}\right) \geq R_{\min}\right] \geq 1 - \epsilon_1, \forall k \tag{43}$$

$$\inf_{\mathbb{P}\in\mathcal{P}} \Pr_{\mathbb{P}}\left[\eta P_s |\hat{h}_k + \Delta_{h_k}|^2 (1 - \alpha_k t_k) \geq E_{C,k}\right] \geq 1 - \epsilon_2, \forall k \tag{44}$$

where $\inf_{\mathbb{P}\in\mathcal{P}} \Pr_{\mathbb{P}}[\cdot]$ denotes the lower bound of the probability under the probability distribution $\mathbb{P}$ and $\mathcal{P}$ is called ambiguity set, which includes all the possible CSI mismatch distributions. $R_{\min}$ represents the throughput threshold for each tag, and $\epsilon_1, \epsilon_2 \in (0, 1)$ is a desired safety factor specified by the practical application or standards. The chance constraints in (43) and (44) satisfy the demand of finding the worst-case distribution among all the possible distributions from the ambiguity set $\mathcal{P}$.

The uncertainty channel estimation errors: Δ_{h_k} and Δ_g in (43) and (44) make the chanceconstraint problem

intractable. To overcome this challenge, we introduce a CVaR-based method, which is known as a good convex approximation of the worst-case chance constraint. Particularly, if the constraint function is concave or quadratic in the random variable, the distributionally robust version of the chance constraints are equivalently to the worst-case CVaR constraint [25], [36], which is described by the following lemma [36].

Lemma 2: For a continuous loss function $L : \mathbb{R}^k \to \mathbb{R}$ that is concave or quadratic in $\boldsymbol{\xi}$. The distributionally robust chance constraint is equivalent to the worst-case constraint, given by [36]

$$\inf_{\mathbb{P}\in\mathcal{P}} \Pr_{\mathbb{P}}\{L(\boldsymbol{\xi}) \le 0\} \ge 1-\epsilon \Longleftrightarrow \sup_{\mathbb{P}\in\mathcal{P}} \mathbb{P}{-}\mathrm{CVaR}_{\epsilon}\{L(\boldsymbol{\xi})\} \le 0 \tag{45}$$

where $\mathbb{P}{-}\mathrm{CVaR}_{\epsilon}\{L(\boldsymbol{\xi})\}$ is denoted as the CVaR of $L(\boldsymbol{\xi})$ at threshold ϵ with respect to $\mathbb{P}$, defined as

$$\mathbb{P}{-}\mathrm{CVaR}_{\epsilon}\{L(\boldsymbol{\xi})\} = \inf_{\beta\in\mathbb{R}} \left\{ \beta + \frac{1}{\epsilon}\mathbb{E}_{\mathbb{P}}\left[(L(\boldsymbol{\xi})-\beta)^{+}\right] \right\}. \tag{46}$$

Moreover, $\mathbb{R}$ is the set of real numbers and $(z)^+ = \max\{0, z\}$, and $\beta \in \mathbb{R}$ is an auxiliary variable introduced by CVaR.
It can be seen from (45) that the distributionally robust version of the chance constraint on the left hand side is equivalent to the worst-case CVaR on the right hand side when the loss function is concave or quadratic in random variable. The worst-case CVaR can be converted into a group of SDP, which will be shown in the following lemma.

Lemma 3: Let $L(\boldsymbol{\xi}) = \boldsymbol{\xi}^{\mathrm{T}}\boldsymbol{Q}\boldsymbol{\xi} + \boldsymbol{q}^{\mathrm{T}}\boldsymbol{\xi} + \boldsymbol{q}^0$ being a quadratic function of $\boldsymbol{\xi}, \forall \boldsymbol{\xi} \in \mathbb{R}^n$. The worst-case CVaR can be computed as [36]

$$\sup_{\mathbb{P}\in\mathcal{P}} \ \mathbb{P}{-}\mathrm{CVaR}_{\epsilon}\{L(\boldsymbol{\xi})\} = \min_{\beta,\boldsymbol{M}} \beta + \frac{1}{\epsilon}\mathrm{Tr}(\boldsymbol{\Omega}\boldsymbol{M}) \tag{47}$$

$$\text{s.t.} \ \ \boldsymbol{M} \in \mathbb{S}^{n+1}, \beta \in \mathbb{R} \tag{48}$$

$$\boldsymbol{M} \succcurlyeq \boldsymbol{0}, \boldsymbol{M} - \begin{bmatrix} \boldsymbol{Q} & \frac{1}{2}\boldsymbol{q} \\ \frac{1}{2}\boldsymbol{q} & \boldsymbol{q}^0 - \beta \end{bmatrix} \succcurlyeq \boldsymbol{0} \tag{49}$$

where $\boldsymbol{M}$ and β are the auxiliary variables and $\boldsymbol{M} \succcurlyeq \boldsymbol{0}$ indicates that $\boldsymbol{M}$ is a positive-semidefinite matrix, $\mathbb{S}^n$ denotes the space of n-dimensional symmetric matrix, and $\boldsymbol{\Omega}$ is a matrix defined as

$$\boldsymbol{\Omega} = \begin{bmatrix} \boldsymbol{\Sigma} + \boldsymbol{\mu}\boldsymbol{\mu}^{\mathrm{T}} & \boldsymbol{\mu} \\ \boldsymbol{\mu}^{\mathrm{T}} & \boldsymbol{1} \end{bmatrix} \tag{50}$$

where $\boldsymbol{\mu} \in \mathbb{R}^n$ and $\boldsymbol{\Sigma} \in \mathbb{S}^n$ are the mean vector and covariance matrix of random vector $\boldsymbol{\xi}$, respectively.

In our case, we define a random vector $\boldsymbol{\xi}_1$, as $\boldsymbol{\xi}_1 = [|\hat{h}_k + \Delta_{h_k}|, |\hat{g} + \Delta_g|]^{\mathrm{T}}$. After the first-order Taylor series expansion of the logarithm function, the loss function L can be expressed as

$$L(h_k, g) = R_{\min}P_s|\hat{g} + \Delta_g|^2 - t_k\alpha_k P_s|f_k|^2|\hat{h}_k + \Delta_{h_k}|^2 + R_{\min}\sigma_R^2 \tag{51}$$

which can be written as a quadratic function in $\boldsymbol{\xi}_1$, as follows:

$$L(\boldsymbol{\xi}_1) = \boldsymbol{\xi}_1^{\mathrm{T}}\boldsymbol{Q}\boldsymbol{\xi}_1 + R_{\min}\sigma_R^2 \tag{52}$$

where

$$\mathbf{Q} = \begin{bmatrix} -\alpha_k P_s|f_k|^2 t_k & 0 \\ 0 & R_{\min}P_s \end{bmatrix}. \tag{53}$$

According to Lemmas 2 and 3, the worst-case chance constraint in (43) can be transformed as the following CVaR constraint:

$$\begin{cases} \beta_1 + \frac{1}{\epsilon_1}\mathrm{Tr}(\Omega_k\mathbf{M}_1) \le 0 \\ \mathbf{M}_1 \in \mathbb{S}^3, \beta_1 \in \mathbb{R} \\ \mathbf{M}_1 \succcurlyeq \mathbf{0}, \mathbf{M}_1 - \begin{bmatrix} \boldsymbol{Q} & \mathbf{0} \\ \mathbf{0} & R_{\min}\sigma_R^2 - \beta_1 \end{bmatrix} \succcurlyeq \mathbf{0} \end{cases} \tag{54}$$

where $\boldsymbol{M}_1$ and β_1 are two auxiliary variables, and

$$\boldsymbol{\Omega}_k = \begin{bmatrix} \boldsymbol{\Sigma}_k + \boldsymbol{\mu}_k\boldsymbol{\mu}_k^{\mathrm{T}} & \boldsymbol{\mu}_k \\ \boldsymbol{\mu}_k^{\mathrm{T}} & \boldsymbol{1} \end{bmatrix} \tag{55}$$

$$\Sigma_k = \begin{bmatrix} \sigma_{h_k,h_k}^2 & 0 \\ 0 & \sigma_{g,g}^2 \end{bmatrix}, \quad \boldsymbol{\mu}_k = \left[\hat{h}_k + \mu_{h_k}, \hat{g} + \mu_g\right]. \tag{56}$$

Similarly, (44) can be also transformed to the CVaR constraint. Let $\boldsymbol{\xi}_2 = |\hat{h}_k + \Delta_{h_k}|$, the loss function of (44) can be expressed as

$$L(\xi_2) = \xi_2^{\mathrm{T}} q \xi_2 + E_{C,k} \tag{57}$$

where

$$q = -\eta P_s(1 - \alpha_k t_k). \tag{58}$$

Using the results in Lemmas 2 and 3, we can derive the CVaR constraint (44), given by

$$\begin{cases} \beta_2 + \frac{1}{\epsilon_2}\mathrm{Tr}\left(\Omega_k'\mathbf{M}_2\right) \le 0 \\ \mathbf{M}_2 \in \mathbb{S}^2, \beta_2 \in \mathbb{R} \\ \mathbf{M}_2 \succcurlyeq \mathbf{0}, \mathbf{M}_2 - \begin{bmatrix} q & 0 \\ 0 & E_{C,k} - \beta_2 \end{bmatrix} \succcurlyeq \mathbf{0} \end{cases} \tag{59}$$

where $\boldsymbol{M}_2$ and β_2 are two auxiliary variables for the EH constraint, and

$$\boldsymbol{\Omega}_k' = \begin{bmatrix} \sigma_{h_k,h_k}^2 + \mu_k'\mu_k'^{T} & \mu_k' \\ \mu_k'^{T} & 1 \end{bmatrix} \tag{60}$$

$$\mu_k' = \hat{h}_k + \mu_{h_k}. \tag{61}$$

Therefore, the original distributionally chance-constrained problem under Scenario 2 can be reformulated as

$$P_2 : \max_{\substack{\boldsymbol{t},\boldsymbol{\alpha},R_{\min}, \\ \boldsymbol{M}_1,\boldsymbol{M}_2,\beta_1,\beta_2}} \quad R_{\min} \tag{62}$$

$$\text{s.t.} \ \ (15), \ (16), \ (17) \tag{63}$$

$$(54), \ (59). \tag{64}$$

Now the chance constraints have been reformulated in a tractable form based on the above two safe approximation methods. However, the throughput and EH constraints are still nonconvex due to the term $\alpha_k t_k$. Next, we will design an alternating algorithm to make the problem solvable.

Algorithm 1 Alternating Optimization Algorithm

Input: Set initial values for $\boldsymbol{t}$ and the terminated threshold Θ.

1: Fix $\boldsymbol{t}$ and solve the subproblem of $\boldsymbol{\alpha}$ to obtain the optimal $\boldsymbol{\alpha}^*$ and optimal throughput *opt_val*.
2: Let $\boldsymbol{\alpha} \leftarrow \boldsymbol{\alpha}^*$, $p_1 \leftarrow opt\_val$.
3: Fix $\boldsymbol{\alpha}$ and solve the subproblem of $\boldsymbol{t}$ to obtain the optimal $\boldsymbol{t}^*$ and optimal throughput *opt_val*.
4: Let $\boldsymbol{t} \leftarrow \boldsymbol{t}^*$, $p_2 \leftarrow opt\_val$.
5: **while** $|p_1 - p_2| > \Theta$, **do**
6: Steps 1, 2, 3 and 4.

Output: $\boldsymbol{t}$, $\boldsymbol{\alpha}$ and *opt_val*.

V. Alternating Optimization Algorithm

In this section, we give an alternating optimization method to address the joint optimization problem of $\boldsymbol{\alpha}$ and $\boldsymbol{t}$, as shown in Algorithm 1. The nonconvexity in problem P_1 and P_2 are caused by the multiplication of α_k and t_k in the constraints. Therefore, the alternating algorithm is designed by fixing the variable t_k first to solve the problem in P_1 and P_2. Then we can obtain the optimal power reflection coefficient $\boldsymbol{\alpha}^* = [\alpha_1^*, \alpha_2^*, \ldots, \alpha_k^*]$ and optimal throughput threshold p_1 by using the off-the-shelf convex optimization solvers, such as CVX. Next, let $\boldsymbol{\alpha} = \boldsymbol{\alpha}^*$, as the fixed variable and we can obtain the optimal backscatter time allocation $\boldsymbol{t}^* = [t_1^*, t_2^*, \ldots, t_k^*]$ as well as the optimal throughput threshold p_2. Repeating in this way, the derived results $\boldsymbol{t}^*$ or $\boldsymbol{\alpha}^*$ at the current step can be used as the fixed value in the next step. The iteration process can be terminated when $|p_1 - p_2|$ is below a certain threshold.

VI. Numerical Results

In this section, we present the simulation results of the proposed chance-constrained optimization problem. The EH efficiency η is 0.5 and the safety factor ϵ_1 and ϵ_2 are set as 0.05. The two parameters E_0 and κ are 7 μJ and 1, respectively. The transmit power P_s and noise σ_R^2 are set to 30 dBm and 10^{-6} W, respectively. The channel coefficient h_k and g are modeled as $10^{-3}d^{-\alpha}h_k$ and $10^{-3}d^{-\alpha}g$, where $\alpha = 3$ is the path loss exponent and d is the distance from PS to the reader or tag. The means of the estimated channel of h_k and g are 1. Finally, the simulation results are based on the CVX package [37]. The iteration termination threshold Θ is set as 10^{-3}. The Monte Carlo runs 10 000 for average.

For comparison, we consider a nonrobust scheme, which treats the estimated CSI of h_k and g as the perfect CSI. Then we can solve the following nonrobust problem:

$$\max_{\boldsymbol{t},\boldsymbol{\alpha},R_{\min}} \quad R_{\min} \tag{65}$$

$$\text{s.t.} \quad \frac{\alpha_k t_k P_s |\hat{h}_k|^2 |f_k|^2}{\sigma_R^2 + |\hat{g}|^2 P_s} \geq R_{\min} \tag{66}$$

$$\eta P_s |\hat{h}_k|^2 (1 - \alpha_k t_k) \geq E_{C,k} \tag{67}$$

$$(15),\ (16),\ (17) \tag{68}$$

by using the alternating optimization algorithm in Algorithm 1. Each iteration is convex and can be solved by CVX.

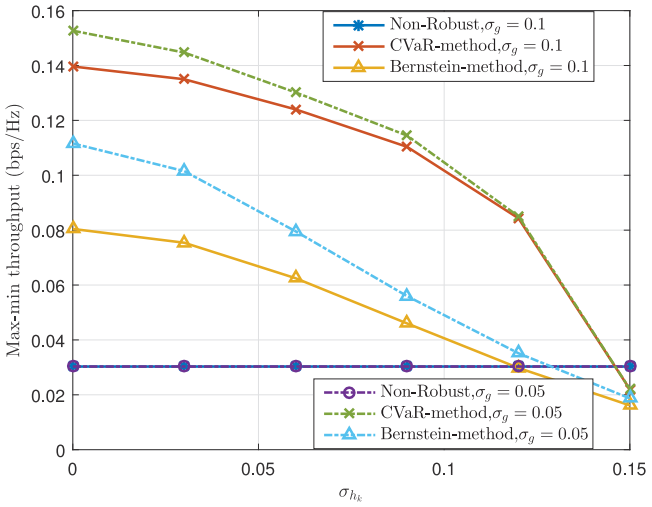

Fig. 4. Max–min throughput versus σ_{h_k} for different optimization methods with non-Gaussian CSI mismatch, $P_s = 1$ dBm, $\sigma_g = 0.1$, or $\sigma_g = 0.05$, $K = 3$.

The distribution of CSI mismatch is non-Gaussian model. We consider the Gaussian mixture model, which is generally used in the non-Gaussian noise approximation [38]. The probability density function of Δ_{h_k} or Δ_g is given as

$$f(\Delta_p) = \sum_{l=1}^{L} \frac{\lambda_{p,l}}{\pi \sigma_{p,l}^2} \exp\left\{ -\frac{|\Delta_p|^2}{\sigma_{p,l}^2} \right\}, p \in \{h_k, g\} \tag{69}$$

where $\sum_{l=1}^{L} \lambda_l = 1$. We set $\lambda_1 = 0.1$ and $\lambda_2 = 0.9$ in the simulation.

Fig. 4 shows the max–min throughput versus the channel estimation error variance σ_{h_k} for different optimization methods. As can be observed, the minimum throughput among tags degrades for both the Bernstein-type-inequality and CVaR-based methods as the quality of CSI decreases. In addition, the max–min throughput for nonrobust scheme remains unchanged as the channel estimation error variance σ_{h_k} and σ_g increase. This is because the nonrobust scheme takes no account of the uncertainty of channels [39], [40]. Moreover, the max–min throughputs of the two proposed methods are larger than that of nonrobust scheme, which indicates the robust schemes can guarantee the resource allocation for the tag with relatively poor channel conditions. It can be also seen from the figure that the CVaR-based method for non-Gaussian CSI errors scenario performs better than the Bernstein-type-inequality-based method.

Fig. 5 depicts the max–min throughput versus the transmit power P_s for the three different optimization scenarios with the channel estimation error variances $\sigma_{h_k} = 0.1$ and $\sigma_g = 0.05$. As we can observe, the max–min throughput is increasing for all the considered schemes with respect to the transmit power P_s. The reason for this phenomenon is that the tag can harvest more energy from the PS with a larger P_s to achieve a higher throughput. However, the max–min throughput increases slowly when P_s exceeds a certain value. This is due to the fact energy consumption for each tag is positively correlated with the individual throughput. In order to meet the

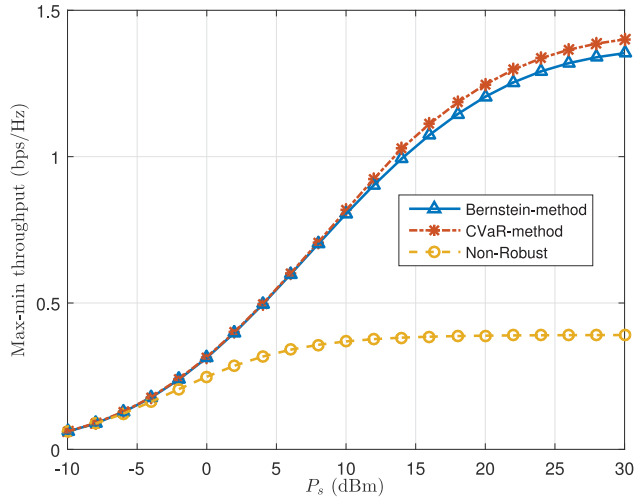

Fig. 5. Max–min throughput versus P_s for different optimization methods with non-Gaussian CSI mismatch, $K = 3$, $\sigma_{h_k} = 0.1$ and $\sigma_g = 0.05$.

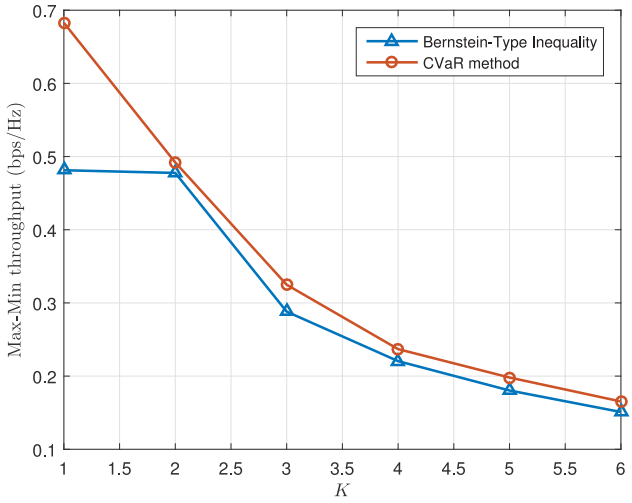

Fig. 7. Max–min throughput versus K for different optimization methods with non-Gaussian CSI mismatch, $P_s = 0$ dBm, $\sigma_{h_k} = 0.1$, and $\sigma_g = 0.05$.

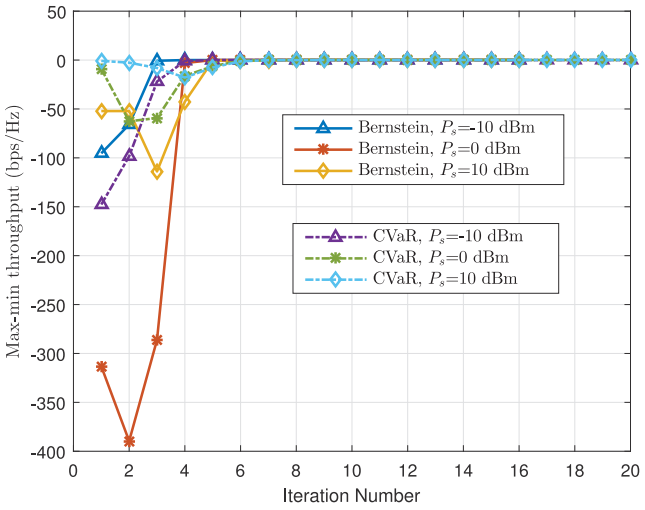

Fig. 6. Max–min throughput versus iteration number for different optimization methods with non-Gaussian CSI mismatch, $\sigma_{h_k} = 0.1$ and $\sigma_g = 0.05$.

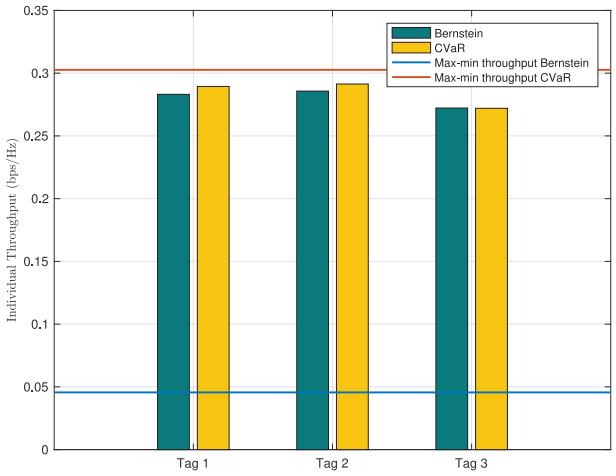

Fig. 8. Individual throughput versus different tags for the non-Gaussian CSI mismatch with $P_s = 0$ dBm, $K = 3$, $\lambda_1 = 0.1$, $\lambda_2 = 0.9$, $\sigma_{h_k} = 0.01$, and $\sigma_g = 0.05$.

EH constraint in (14), the throughput cannot monotonically increase with the respect to the transmit power.

Fig. 6 demonstrates the convergence behavior of the proposed alternating optimization algorithm in Algorithm 1 for the proposed robust methods with $P_s = 0$ dBm, $\sigma_{h_k} = 0.1$, and $\sigma_g = 0.05$. It can be observed that all the proposed method can converge within only 16 iterations, which indicates the practical applicability of the algorithm. Moreover, the convergence speed of the Bernstein-type-inequality method is faster than that of the CVaR-based method. This is due to the fact that the CVaR method considering the worst-case scenario among all the distributions, which is more complex compared to the Bernstein-type-inequality method under the Scenario 1. The iteration number increases as the transmit power increases.

Fig. 7 depicts the max–min throughput versus the number of tags. As the number of tags increases, the max–min throughput among all the tags becomes smaller. The constraint in (13) is supposed to guarantee the throughput requirement for all the tags despite their potentially poor channel conditions. So, the max–min throughput is limited by the tag with the worst channel condition. As the number of tags increases in the system, the probability of a tag with poor channel condition increases, which leads to the decrease of the max–min throughput.

In Fig. 8, we can find the throughput of each tag under the CVaR method is larger than that under the Bernstein-type-inequality. This is because we assume the CSI error is Gaussian when we use the Bernstein-type-inequality method. The performance of the Bernstein-type-inequality-based method would degrade when the distribution of CSI error becomes non-Gaussian. Moreover, we can see the individual throughput of each tag cannot meet the minimum throughput requirements. The robustness of the Bernstein-type-inequality method is not good as the CVaR method.

In Fig. 9, we present the sum throughput versus the transmit power P_s when the distribution of channel estimation errors are the non-Gaussian mixture model. We can find that the sum throughput is monotonically increasing with respect to

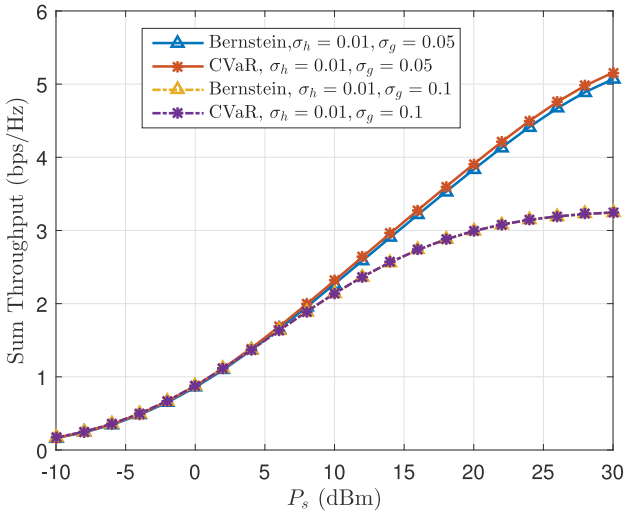

Fig. 9. Sum throughput versus P_s for the non-Gaussian CSI mismatch with $P_s = 0$ dBm, $K = 3$, $\lambda_1 = 0.1$, $\lambda_2 = 0.9$.

the transmit power for all considered methods. This is because each of the tags can harvest more energy when the transmit power is increased. Moreover, the CVaR-based method can achieve better performance than that of Bernstein-type-inequality-based method. The sum throughput degrades as the channel error estimation error variance σ_g increases. In addition, the sum throughput gap between CVaR method and Bernstein-type-inequality becomes smaller for a larger value of σ_g, which indicates that CVaR method is sensitive to the channel estimation error with a large variance.

VII. Conclusion

In this paper, we have proposed a chance-constrained optimization problem to deal with the imperfection of CSI for the design of multitag ABSs. We propose a joint backscatter time allocation and power reflection coefficient optimization algorithm for maximizing the minimum individual throughput among all the tags. We adopt the Bernstein-type-inequality-based method to solve the chance constraint problem for the Gaussian distribution of CSI errors. Furthermore, we utilize the CVaR-based method to reformulate the distributionally robust version of the chance constraint into a tractable alternative. An effective alternating algorithm is developed for solving the transformed problem. Simulation results show that the robust design can cause a decrease of the max–min throughput and reveal the existence of tradeoff between the max–min throughput and the robustness. Moreover, CVaR-based method can effectively solve the worst-case chance constrained problem and outperform the Bernstein-type-inequality method for the non-Gaussian channel estimation errors.

Appendix A
Proof of Equation (19)

The covariance matrix of $\boldsymbol{v}_k$ is defined as

$$\boldsymbol{C}_k = \begin{bmatrix} E\big[(\Delta_{h_k} - \mu_{h_k})(\Delta_{h_k} - \mu_{h_k})\big] & E\big[(\Delta_{h_k} - \mu_{h_k})(\Delta_g - \mu_g)\big] \\ E\big[(\Delta_g - \mu_g)(\Delta_{h_k} - \mu_{h_k})\big] & E\big[(\Delta_g - \mu_g)(\Delta_g - \mu_g)\big] \end{bmatrix} \tag{70}$$

where

$$E\big[(\Delta_i - \mu_i)(\Delta_j - \mu_j)\big] = E\big[\Delta_i \Delta_j\big] - \mu_i \mu_j, i, j \in \{h_k, g\}. \tag{71}$$

According to (10), we have $\mu_{h_k} = \mu_g = 0$. The elements of the main diagonal in $\boldsymbol{C}_k$ are the variance of Δ_{h_k} and Δ_g, i.e., $\sigma_{h_k}^2$ and σ_g^2, respectively. Moreover, Δ_{h_k} and Δ_g are independent with each other. It is easy to derive the elements of back diagonal as 0.

Appendix B
Proof of Equation (20)

We use the first-order Taylor series expansion of the logarithm function, then (13) can be written as

$$\Pr\left[\frac{\alpha_k t_k P_s |\hat{h}_k + \Delta_{h_k}|^2 |f_k|^2}{\sigma_R^2 + |\hat{g} + \Delta_g|^2 P_s} \geq R_{\min}\right] \geq 1 - \epsilon_1, \forall k \tag{72}$$

where

$$\left|\hat{h}_k + \Delta_{h_k}\right|^2 = |\Delta_{h_k}|^2 + 2\mathrm{Re}\left\{\Delta_{h_k}^{\mathrm{H}} \hat{h}_k\right\} + |\hat{h}_k|^2 \tag{73}$$

$$|\hat{g} + \Delta_g|^2 = |\Delta_g|^2 + 2\mathrm{Re}\left\{\Delta_g^{\mathrm{H}} \hat{g}\right\} + |\hat{g}|^2. \tag{74}$$

For a given vector $\boldsymbol{x} = [x_1, x_2]$, if

$$F(x_1, x_2) = a x_1^2 + b x_2^2 + c x_1 x_2 \tag{75}$$

then the quadratic form of $\boldsymbol{x}$ can be written as

$$F(\boldsymbol{x}) = \boldsymbol{x}^{\mathrm{T}} \Phi \boldsymbol{x} \tag{76}$$

where

$$\Phi = \begin{bmatrix} a & \frac{c}{2} \\ \frac{c}{2} & b \end{bmatrix}. \tag{77}$$

Based on this fact, we can derive the result in (20).

References

[1] C. Konstantopoulos, E. Koutroulis, N. Mitianoudis, and A. Bletsas, "Converting a plant to a battery and wireless sensor with scatter radio and ultra-low cost," *IEEE Trans. Instrum. Meas.*, vol. 65, no. 2, pp. 388–398, Feb. 2016.

[2] B. Lyu, H. Guo, Z. Yang, and G. Gui, "Throughput maximization for hybrid backscatter assisted cognitive wireless powered radio networks," *IEEE Internet Things J.*, vol. 5, no. 3, pp. 2015–2024, Jun. 2018.

[3] N. V. Huynh, D. T. Hoang, X. Lu, D. Niyato, P. Wang, and D. I. Kim, "Ambient backscatter communications: A contemporary survey," *IEEE Commun. Surveys Tuts.*, vol. 20, no. 4, pp. 2889–2922, 4th Quart., 2018.

[4] Y. Zhang, F. Gao, L. Fan, X. Lei, and G. K. Karagiannidis, "Backscatter communications over correlated Nakagami-*m* fading channels," *IEEE Trans. Commun.*, vol. 67, no. 2, pp. 1693–1704, Feb. 2019.

[5] J. Kimionis, A. Bletsas, and J. N. Sahalos, "Increased range bistatic scatter radio," *IEEE Trans. Commun.*, vol. 62, no. 3, pp. 1091–1104, Mar. 2014.

[6] S. H. Kim and D. I. Kim, "Hybrid backscatter communication for wireless-powered heterogeneous networks," *IEEE Trans. Wireless Commun.*, vol. 16, no. 10, pp. 6557–6570, Oct. 2017.

[7] N. Fasarakis-Hilliard, P. N. Alevizos, and A. Bletsas, "Coherent detection and channel coding for bistatic scatter radio sensor networking," *IEEE Trans. Commun.*, vol. 63, no. 5, pp. 1798–1810, May 2015.

[8] V. Liu, A. Parks, V. Talla, S. Gollakota, D. Wetherall, and J. R. Smith, "Ambient backscatter: Wireless communication out of thin air," in *Proc. ACM SIGCOMM*, Hong Kong, Aug. 2013, pp. 39–50.

[9] G. Zhang, Y. Zhang, and W. Kang, "Low-complexity channel estimation for the UHF MIMO-RFID systems with optimal training," *Int. J. Adv. Comput. Technol.*, vol. 4, no. 1, pp. 387–394, Jan. 2012.
[10] S. Ma, G. Wang, R. Fan, and C. Tellambura, "Blind channel estimation for ambient backscatter communication systems," *IEEE Commun. Lett.*, vol. 22, no. 6, pp. 1296–1299, Jun. 2018.
[11] D. Mishra and E. G. Larsson, "Optimal channel estimation for reciprocity-based backscattering with a full-duplex MIMO reader," *IEEE Trans. Signal Process.*, vol. 67, no. 6, pp. 1662–1677, Mar. 2019.
[12] Y. Karimi, Y. Huang, A. Athalye, S. Das, P. Djurić, and M. Stanaćević, "Passive wireless channel estimation in RF tag network," in *Proc. IEEE Int. Symp. Circuits Syst. (ISCAS)*, Sapporo, Japan, May 2019, pp. 1–5.
[13] C. He, Z. J. Wang, and C. Miao, "Query diversity schemes for backscatter RFID communications with single-antenna tags," *IEEE Trans. Veh. Technol.*, vol. 66, no. 8, pp. 6932–6941, Aug. 2017.
[14] Z. Chu, F. Zhou, Z. Zhu, R. Q. Hu, and P. Xiao, "Wireless powered sensor networks for Internet of Things: Maximum throughput and optimal power allocation," *IEEE Internet Things J.*, vol. 5, no. 1, pp. 310–321, Feb. 2018.
[15] D. Li and Y.-C. Liang, "Adaptive ambient backscatter communication systems with MRC," *IEEE Trans. Veh. Technol.*, vol. 67, no. 12, pp. 12352–12357, Dec. 2018.
[16] D. Li, W. Peng, and Y.-C. Liang, "Hybrid ambient backscatter communication systems with harvest-then-transmit protocols," *IEEE Access*, vol. 6, pp. 45288–45298, 2018.
[17] R. Duan, R. Jäntti, H. Yiğitler, and K. Ruttik, "On the achievable rate of bistatic modulated rescatter systems," *IEEE Trans. Veh. Technol.*, vol. 66, no. 10, pp. 9609–9613, Oct. 2017.
[18] S. Gong, X. Huang, J. Xu, W. Liu, P. Wang, and D. Niyato, "Backscatter relay communications powered by wireless energy beamforming," *IEEE Trans. Commun.*, vol. 66, no. 7, pp. 3187–3200, Jul. 2018.
[19] Q. Yao, A. Huang, H. Shan, and T. Q. S. Quek, "WET-enabled passive communication networks: Robust energy minimization with uncertain CSI distribution," *IEEE Trans. Wireless Commun.*, vol. 17, no. 1, pp. 282–295, Jan. 2018.
[20] T. A. Le, Q.-T. Vien, H. X. Nguyen, D. W. K. Ng, and R. Schober, "Robust chance-constrained optimization for power-efficient and secure SWIPT systems," *IEEE Trans. Green Commun. Netw.*, vol. 1, no. 3, pp. 333–346, Sep. 2017.
[21] K.-Y. Wang, A. M.-C. So, T.-H. Chang, W.-K. Ma, and C.-Y. Chi, "Outage constrained robust transmit optimization for multiuser MISO downlinks: Tractable approximations by conic optimization," *IEEE Trans. Signal Process.*, vol. 62, no. 21, pp. 5690–5705, Nov. 2014.
[22] B. Li, Y. Rong, J. Sun, and K. L. Teo, "A distributionally robust linear receiver design for multi-access space-time block coded MIMO systems," *IEEE Trans. Wireless Commun.*, vol. 16, no. 1, pp. 464–474, Jan. 2017.
[23] Q. Li, A. M.-C. So, and W.-K. Ma, "Distributionally robust chance-constrained transmit beamforming for multiuser MISO downlink," in *Proc. IEEE Int. Conf. Acoust. Speech Signal Process. (ICASSP)*, Florence, Italy, May 2014, pp. 3479–3483.
[24] B. Li, X. Qian, J. Sun, K. L. Teo, and C. Yu, "A model of distributionally robust two-stage stochastic convex programming with linear recourse," *Appl. Math. Model.*, vol. 58, pp. 86–97, Jun. 2018.
[25] B. Li, Y. Rong, J. Sun, and K. L. Teo, "A distributionally robust minimum variance beamformer design," *IEEE Signal Process. Lett.*, vol. 25, no. 1, pp. 105–109, Jan. 2018.
[26] B. Li, J. Sun, H. Xu, and M. Zhang, "A class of two-stage distributionally robust stochastic games," *J. Ind. Manag. Optim.*, Jan. 2019.
[27] Y. Dong, M. J. Hossain, and J. Cheng, "Joint power control and time switching for SWIPT systems with heterogeneous QoS requirements," *IEEE Commun. Lett.*, vol. 20, no. 2, pp. 328–331, Feb. 2016.
[28] B. Li and Y. Rong, "Joint transceiver optimization for wireless information and energy transfer in non-regenerative MIMO relay systems," *IEEE Trans. Veh. Technol.*, vol. 67, no. 9, pp. 8348–8362, Sep. 2018.
[29] B. Li and Y. Rong, "AF MIMO relay systems with wireless powered relay node and direct link," *IEEE Trans. Commun.*, vol. 66, no. 4, pp. 1580–1589, Apr. 2018.
[30] G. Yang, D. Yuan, Y.-C. Liang, R. Zhang, and V. C. M. Leung, "Optimal resource allocation in full-duplex ambient backscatter communication networks for wireless-powered IoT," *IEEE Internet Things J.*, vol. 6, no. 2, pp. 2612–2625, Apr. 2019.
[31] T. Wang and L. Vandendorpe, "On the optimum energy efficiency for flat-fading channels with rate-dependent circuit power," *IEEE Trans. Commun.*, vol. 61, no. 12, pp. 4910–4921, Dec. 2013.
[32] G. Wang, F. Gao, R. Fan, and C. Tellambura, "Ambient backscatter communication systems: Detection and performance analysis," *IEEE Trans. Commun.*, vol. 64, no. 11, pp. 4836–4846, Nov. 2016.
[33] J. Qian, F. Gao, G. Wang, S. Jin, and H. Zhu, "Noncoherent detections for ambient backscatter system," *IEEE Trans. Wireless Commun.*, vol. 16, no. 3, pp. 1412–1422, Mar. 2017.
[34] S. Ma, M. Hong, E. Song, X. Wang, and D. Sun, "Outage constrained robust secure transmission for MISO wiretap channels," *IEEE Trans. Wireless Commun.*, vol. 13, no. 10, pp. 5558–5570, Oct. 2014.
[35] D. Darsena, G. Gelli, and F. Verde, "Joint channel estimation, interference cancellation, and data detection for ambient backscatter communications," in *Proc. IEEE Int. Workshop Signal Process. Adv. Wireless Commun. (SPAWC)*, Kalamata, Greece, Jun. 2018, pp. 1–5.
[36] S. Zymler, D. Kuhn, and B. Rustem, "Distributionally robust joint chance constraints with second-order moment information," *Math. Program.*, vol. 137, nos. 1–2, pp. 167–198, Feb. 2013.
[37] M. Grant and S. Boyd. (Apr. 2011). *CVX: MATLAB Software for Disciplined Convex Programming*. [Online]. Available: http://cvxr.com/cvx
[38] R. J. Kozick and B. M. Sadler, "Maximum-likelihood array processing in non-Gaussian noise with Gaussian mixtures," *IEEE Trans. Signal Process.*, vol. 48, no. 12, pp. 3520–3535, Dec. 2000.
[39] C. Xing, S. Ma, Z. Fei, Y.-C. Wu, and H. V. Poor, "A general robust linear transceiver design for multi-hop amplify-and-forward MIMO relaying systems," *IEEE Trans. Signal Process.*, vol. 61, no. 5, pp. 1196–1209, Mar. 2013.
[40] C. Xing, S. Ma, and Y.-C. Wu, "Robust joint design of linear relay precoder and destination equalizer for dual-hop amplify-and-forward MIMO relay systems," *IEEE Trans. Signal Process.*, vol. 58, no. 4, pp. 2273–2283, Apr. 2010.

Yu Zhang received the B.Eng. degree in communication engineering from Shandong University, Jinan, China, in 2016. She is currently pursuing the Ph.D. degree with the Department of Automation, Tsinghua University, Beijing, China.

She is currently a visiting Ph.D. student with the Department of Electrical and Computer Engineering, University of Houston, Houston, TX, USA. Her current research interests include performance analysis, backscatter communications, optimization, deep reinforcement learning, and UAV.

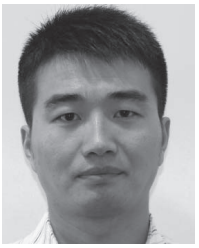

Bin Li (M'18–SM'18) received the bachelor's degree in automation and the master's degree in control science and engineering from the Harbin Institute of Technology, Harbin, China, in 2005 and 2008, respectively, and the Ph.D. degrees in mathematics and in statistics from Curtin University, Perth, WA, Australia, in 2011.

From 2012 to 2014, he was a Research Associate with the School of Electrical, Electronic and Computer Engineering, University of Western Australia, Perth. From 2014 to 2017, he was a Research Fellow with the Department of Mathematics and Statistics, Curtin University. He is currently a Research Professor with the College of Electrical Engineering, Sichuan University, Chengdu, China. His current research interests include signal processing, wireless communications, optimization, and optimal control.

Feifei Gao (M'09–SM'14) received the B.Eng. degree from Xi'an Jiaotong University, Xi'an, China, in 2002, the M.Sc. degree from McMaster University, Hamilton, ON, Canada, in 2004, and the Ph.D. degree from the National University of Singapore, Singapore, in 2007.

He was a Research Fellow with the Institute for Infocomm Research, A*STAR, Singapore, in 2008 and an Assistant Professor with the School of Engineering and Science, Jacobs University, Bremen, Germany, from 2009 to 2010. In 2011, he joined the Department of Automation, Tsinghua University, Beijing, China, where he is currently an Associate Professor. He has authored/coauthored over 120 refereed IEEE journal papers and over 120 IEEE conference proceeding papers. His current research interests include communication theory, signal processing for communications, array signal processing, and convex optimizations, with particular interests in MIMO techniques, multicarrier communications, cooperative communication, and cognitive radio networks.

Dr. Gao has served as an Editor for the IEEE TRANSACTIONS ON WIRELESS COMMUNICATIONS, the IEEE SIGNAL PROCESSING LETTERS, the IEEE COMMUNICATIONS LETTERS, the IEEE WIRELESS COMMUNICATIONS LETTERS, the *International Journal on Antennas and Propagations*, and *China Communications.* He has also served as the Symposium Co-Chair for the 2019 IEEE Conference on Communications, the 2018 IEEE Vehicular Technology Conference Spring, the 2015 ICC, the 2014 IEEE Global Communications Conference, and the 2014 IEEE VTC Fall, and as a technical committee member for many other IEEE conferences.

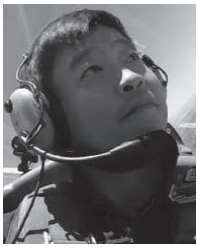

Zhu Han (S'01–M'04–SM'09–F'14) received the B.S. degree in electronic engineering from Tsinghua University, Beijing, China, in 1997 and the M.S. and Ph.D. degrees in electrical and computer engineering from the University of Maryland at College Park, College Park, MD, USA, in 1999 and 2003, respectively.

From 2000 to 2002, he was a Research and Development Engineer with JDSU, Germantown, MD, USA. From 2003 to 2006, he was a Research Associate with the University of Maryland at College Park. From 2006 to 2008, he was an Assistant Professor with Boise State University, Boise, ID, USA. He is currently a John and Rebecca Moores Professor with the Electrical and Computer Engineering Department and the Computer Science Department, University of Houston, Houston, TX, USA. He is also the Chair Professor with National Chiao Tung University, Hsinchu, Taiwan. His current research interests include wireless resource allocation and management, wireless communications and networking, game theory, big data analysis, security, and smart grid.

Dr. Han was a recipient of the NSF Career Award in 2010, the Fred W. Ellersick Prize of the IEEE Communication Society in 2011, the EURASIP Best Paper Award for the *Journal on Advances in Signal Processing* in 2015, the IEEE Leonard G. Abraham Prize in the field of Communications Systems (Best Paper Award in the IEEE JOURNAL ON SELECTED AREAS IN COMMUNICATIONS) in 2016, and several best paper awards in IEEE conferences. He is currently an IEEE Communications Society Distinguished Lecturer in 2015–2018. He is 1% Highly Cited Researcher since 2017 according to Web of Science.